System-Level Robust Design Optimization of a Switched Reluctance Motor Drive System Considering Multiple Driving Cycles

Kaikai Diao, *Student Member, IEEE*, Xiaodong Sun, *Senior Member, IEEE*, Gang Lei, *Member, IEEE*, Gerd Bramerdorfer, *Senior Member, IEEE*, Youguang Guo, *Senior Member, IEEE*, and Jianguo Zhu, *Senior Member, IEEE*

***Abstract*—In this paper, a novel system-level robust design optimization method is presented to improve the performance of switched reluctance motor (SRM) drive systems under multiple operating conditions. Based on typical driving cycles of electric vehicles (EVs), five typical driving modes of the SRM are determined. The optimization objectives in each driving mode are established. The significant parameters of the motor and controller of each driving mode are selected as the optimization variables by using the sensitivity analysis. In order to simplify the optimization process, correlation analysis is performed to determine the coherence of the objective functions of all driving modes. Then, a sequential Taguchi method is applied to find an optimal design which is less sensitive to the noise factors. To verify the effectiveness of the proposed method, an SRM drive system applied in EVs with a 12/10 SRM and angle position control method is investigated. It is found that the proposed method can significantly reduce the torque ripple and improve the comprehensive performance. Finally, a 12/10 SRM is prototyped and tested to validate the simulation results.**

***Index Terms*—Multiobjective optimization, robust design, switched reluctance motor (SRM), Taguchi method.**

I. Introduction

SWITCHED reluctance motors (SRMs) are a type of doubly salient machines without permanent magnets (PMs), which have drawn considerable attention due to their inherent advantages of low manufacturing cost, high robustness, and fast dynamic response [1], [2]. They have become a feasible alternative to conventional electric machines in applications, such as electric vehicles (EVs) and hybrid EVs (HEVs) [3], [4], [5]. For instance, as reported in [3], a 50-kW continuous power rated SRM was designed based on torque-speed curve for off-road vehicle application. In [4], a comprehensive optimization which combined static and transient analysis was presented for a segmental rotor SRM. The proposed SRM was designed to maximize efficiency with the aim of achieving performance equivalent to that of interior permanent magnet motor utilized in Nissan's leaf EV. Moreover, load test results over the entire speed range of the SRM designed for HEV application was presented in [5].

To achieve the desired performance, optimization is a necessary step for SRMs. Optimization methods in previous work can be divided into single objective and multiobjective optimization scenarios [6], [7]. The single objective optimization method is done to address only one performance index with the potential unfavorable downgrading of other performance indices [8], [9]. Thus, the multiobjective optimization method is preferred to accommodate the requirements for different applications [10]. For example, in [11], a multiobjective optimization design method which contains six objectives was conducted for an SRM designed for low-speed EVs. The stator pole arc, rotor pole arc, rotor radius, and the air gap of SRM are selected as the design parameters. In [12], an in-wheel SRM was designed by using a multiobjective differential evolution algorithm. Six geometry variables, i.e., stator pole angle, rotor pole angle, stator pole height, rotor pole height, stator yoke length, and rotor yoke length are employed to optimize the static torque, torque per motor lamination volume, and efficiency.

Aside from the geometry design aspect, multiobjective optimization has also been performed on the control aspect of SRMs. The PI controller gains, the turn on and turn off angles can also be selected as design parameters [13], [14]. To obtain the best performance of the drive system, the geometry and control variables should be designed and optimized at the system level rather than the component level [15], [16]. Although the system-level optimization methods have been applied to the optimization of PM motors [17], not much work has been reported about its application for SRM drives optimization.

There are many unavoidable noise factors for the design

Manuscript received February 7, 2020; revised May 5, 2020 and June 13, 2020; accepted July 12, 2020. This work was supported by the National Natural Science Foundation of China under Project 51875261, the Natural Science Foundation of Jiangsu Province of China under Projects BK20180046 and BK20170071, the "Qinglan project" of Jiangsu Province, the Key Project of Natural Science Foundation of Jiangsu Higher Education Institutions under Project 17KJA460005, and the Postgraduate Research & Practice Innovation Program of Jiangsu Province under Project KYCX20_2844. *(Kaikai Diao and Xiaodong Sun contributed equally to this work.)* (*Corresponding author: Xiaodong Sun*.)

K. Diao and X. Sun are with the Automotive Engineering Research Institute, Jiangsu University, Zhenjiang 212013, China (email: diaokaikai@163.com, xdsun@ujs.edu.cn).

G. Lei and Y. Guo are with the School of Electrical and Data Engineering, University of Technology Sydney, NSW 2007, Australia (e-mail: Gang.Lei@uts.edu.au, Youguang.Guo-1@uts.edu.au).

Gerd Bramerdorfer is with the Department of Electrical Drives and Power Electronics, Johannes Kepler University Linz, Austria (email: gerd.bramerdorfer@jku.at)

J. Zhu is with the School of Electrical and Information Engineering, University of Sydney, NSW, 2006, Australia (e-mail: jianguo.zhu@sydney.edu.au).

variables of SRMs due to manufacturing tolerances and material diversity [18], [19]. These variations will greatly affect the performance of SRMs. Thus, the robust optimization method which takes the manufacturing quality into account is an effective way to handle this problem. The six-sigma methodology is generally used to develop products to meet the needs with very low defect levels, and it can achieve 3.4 defects per million. As reported in [20], a multilevel robust optimization framework is presented to meet the six-sigma level based on finite element analysis (FEA). However, it requires abundant data achieved from FEA and complicated algorithms, which is time-consuming and will increase the run time of the motor optimization. Taguchi method is an efficient robust approach since it does not use complex algorithms and the number of required finite element simulations can be significantly reduced by using an orthogonal array [21], [22].

Generally, the above-mentioned optimization techniques considering either single or multiple objectives along with a system-level approach and further quantifying the designs' robustness are mainly performed for single load point analysis. As reported in [23], the optimization process for the in-wheel SRM in EVs was only conducted under rated operation condition. However, for the application of EVs, manifold driving conditions are required during operation, such as frequent start and stop, acceleration and deceleration, climbing, and high-speed cruise [24], [25]. In [26], the energy efficiency of the traction machine over the driving cycle was characterized by evaluating a number of representative points. The overall design optimization for SRMs applied in EVs are very challenging to meet the requirements under different driving conditions [27], [28]. Consequently, SRMs designed for EV application should possess the capability of multimode operation.

In this paper, this requirement is incorporated into the multiobjective robust optimization under the consideration of both geometry and control variables. A novel system-level robust design optimization method is proposed for SRM in the application of EVs. The remainder of this paper is organized as follows. Section II presents the proposed system-level robust optimization method considering multiple driving cycles. Both the sensitive variables in geometry and control aspects are selected as the optimization variables. The design levels of optimization variables and noise factors are determined to facilitate applying the Taguchi method. In Section III, a design example of a 12/10 SRM applied in EVs is investigated. The concept for multimode evaluation is proposed, and the sensitivity analysis, correlation analysis and sequential Taguchi method are implemented. Experimental validations are given in Section IV, followed by the conclusion in Section V.

II. System-Level Robust Optimization Method Considering Multiple Driving Cycles

A. Multiple driving cycles

Fig. 1 shows the typical new European driving cycles (NEDC) [24]. It can be seen that several different driving modes, i.e. starting and stop, normal cruise, acceleration, high-speed cruise, and climbing, frequently occur in the NEDC. Thus, it is essential to consider the therewith associated manifold SRM operating points during the optimization process.

The relationship among the driving modes, design requirements and motor operation is shown in Fig. 2. According to the different driving modes, the designed SRM should meet the requirements for the whole operating range. It should be noted that one driving cycle may put forward multiple design requirements, and one design requirement may be applied to several driving modes. For example, the normal cruise of driving cycles puts forward high torque, low torque ripple and high efficiency of the motor. Besides, the low torque ripple is correlated to the driving modes like normal operation, open-circuit fault and short-circuit fault.

Since different requirements are needed in different driving modes, it is meaningful to propose a multiobjective optimization method for the optimization of the multiple driving modes. Besides, for the application in EVs, the performance evaluation of the motor drive system is necessary, and the manufacturing tolerance should also be considered during the whole optimization process. Thus, the aim of this paper is to propose a design optimization method which integrates the concept of multiple driving modes, system level optimization, and robust design.

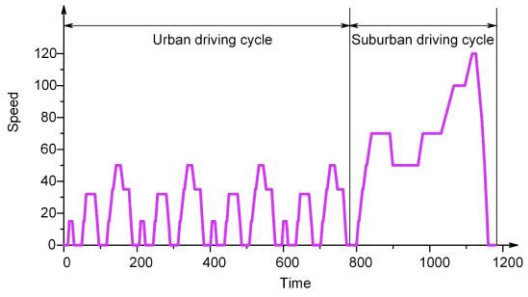

Fig. 1. NEDC driving cycle.

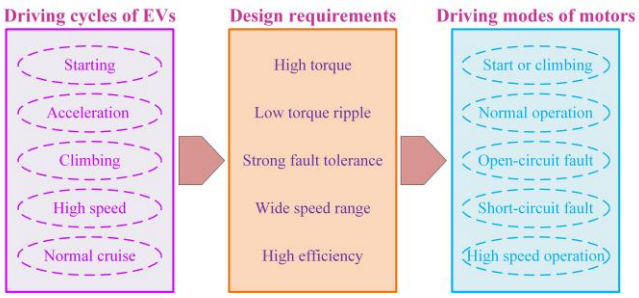

Fig. 2. Relationships among driving cycles, design requirements and the operating range of SRMs.

B. System-level robust optimization

Fig. 3 shows in brief the procedures for the proposed new system-level robust optimization method for electrical drive systems applied in EVs. This kind of system-level robust optimization method has simultaneously taken the driving cycles of EVs, the geometry and control parameters of the SRM drive system, and the manufacturing tolerances into consideration. It can be subdivided into the next four steps.

Step 1: Initial design

In this step, the driving cycles of EVs are determined first according to road condition. Then, the requirements of EVs can be defined. Based on the driving cycles and requirements, the operation of the motor can be classified into different modes. Finally, an initial design can be derived based on the requirements in each mode.

Step 2: Sensitivity analysis

Compared with the optimization for one operating point, the proposed approach includes one sensitivity analysis per each driving mode. The significant variables of the drive system in each mode can be selected according to the results of sensitivity analysis.

Step 3: Taguchi robust optimization

In this step, the objective function for all the driving modes is defined at first. The levels of optimization variables and noise factors are determined to set up the orthogonal array. Then, the required evaluations based on finite element models (FEMs) are specified according to the orthogonal array, which helps greatly reduce the overall number of necessary simulations. Finally, the optimal design can be selected based on the analysis of the results.

Step 4: Performance evaluation

The motor performance of the optimal design is evaluated by FEA. Consequently, experiments about the investigated driving modes are carried out to verify the simulation results.

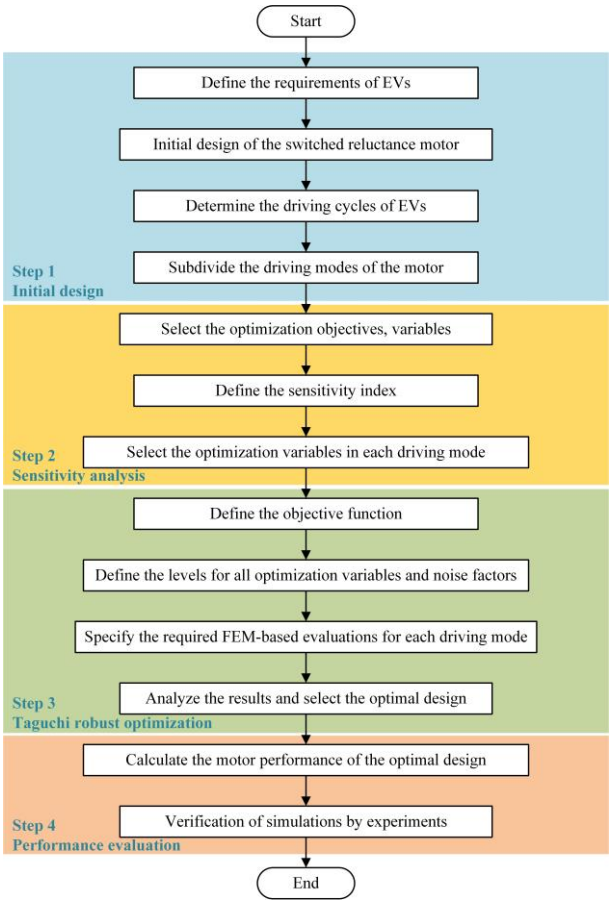

Fig. 3. Procedures of the proposed optimization method.

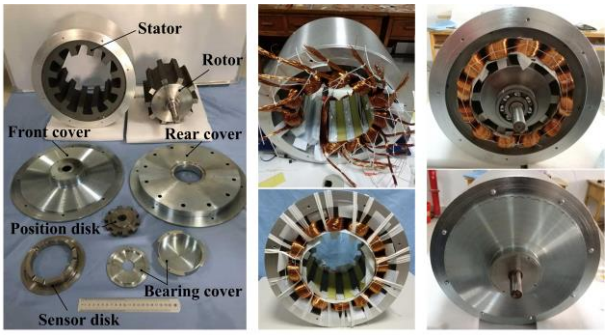

Fig. 4. The prototype of the SRM.

TABLE I
SPECIFICATIONS OF THE SRM

Rated power	75 kW
Peak power	110 kW
Rated speed	6000 r/min
Maximum speed	12000 r/min
DC link voltage	384 V
Efficiency	≥ 85% at rated speed
Cooling type	Water-cooling

TABLE II
INITIAL DESIGN VALUES

Parameter	Description	Unit	Value
D_{so}	Stator outer diameter	mm	310
l_s	Stack length	mm	190
D_{ro}	Rotor outer diameter	mm	204
β_s	Stator pole arc	deg.	13.5
β_r	Rotor pole arc	deg.	12
h_{cs}	Stator yoke thickness	mm	21
h_{cr}	Rotor yoke thickness	mm	20
g	Length of air gap	mm	0.5
n	Number of turns	-	26
θ_{on}	Turn-on angle	deg.	-5
θ_{off}	Turn-off angle	deg.	11

III. A DESIGN EXAMPLE

In this example, a 12/10 six-phase SRM is designed for the application in EVs. The specifications of the SRM are listed in Table I, according to which the motor should feature a torque of 120 Nm at the rated speed of 6000 r/min, while providing a minimal efficiency of 85%. Fig. 4 shows the prototype and the assembly process of the SRM. The SRM is mainly comprised of stator core with 12 poles wrapped by windings, and rotor core with 10 poles without any coil, magnets, or squirrel cage. It has six phase windings, and each phase winding consists of two coils wound on the opposite two poles of the stator. These two coils are connected in parallel. The initial design values are listed in Table II. The external dimensions of the motor are fixed as constant values due to the limitation of the space. Thus, the stator outer diameter and stack length are specified to 310 and 190 mm, respectively.

The whole discussion of the optimization method is based on identifying different driving modes based on the considered driving cycle. Thus, this categorization is considered as first step. Consequently, the sensitivity analysis based on FEMs is performed to select the significant variables for each driving

mode. Then, since some objectives in different driving modes may be positively correlated, the correlation analysis is conducted to determine these objectives and select only one objective to substitute all the positively correlated objectives, which will significantly reduce the computational cost. Finally, a sequential Taguchi optimization method which holds the advantage of both Taguchi method and sequential optimization strategy is carried out to find the optimal solution for multimode application based on FEMs.

C. Multimode concept

The driving modes of the SRM applied in EVs can be categorized into the following five types according to the driving cycle and design requirements shown in Figs. 1 and 2.

1) *Mode 1*: Normal operation

In this mode, the focus should be laid on the performances of torque, losses, and torque ripple. Thus, these three objectives are set as the optimization objectives. The objective function in this mode is to maximize the average torque, minimize the loss and torque ripple, which is given as

$$\text{Objectives}: \begin{cases} \max T_{avg\_1} \\ \min P_{loss\_1} \\ \min T_{ripple\_1} \end{cases} \tag{1}$$

where T_{avg_1}, P_{loss_1}, and T_{ripple_1} are the output torque, loss, and torque ripple in mode 1.

2) *Mode 2*: Start or climbing

The start and stop operation conditions always occur during urban driving, as shown in Fig. 1. In the mode of startup operation of the motor, high torque is the foremost requirement and it is set as the operation objective in this mode. The driving cycle of the climbing is similar to the start operation, which also requires high output torque. Thus, the mode of start and climbing is combined as one single independent driving mode. The objective function in this mode is given as

$$\text{Objective}: \ \max T_{avg\_2} \tag{2}$$

where T_{avg_2} is the output torque in mode 2.

3) *Mode 3*: Open circuit fault operation

In this mode, the torque ripple is the major concern due to the operation reliability. Thus, the torque ripple is selected as the optimization objective. The objective function in this mode is given as

$$\text{Objective}: \ \min T_{ripple\_3} \tag{3}$$

where T_{ripple_3} is the torque ripple in mode 3.

4) *Mode 4*: Short circuit fault operation

Since due to vibration the insulation of the copper wire might get damaged when the motor runs for long time in this operating mode. The most likely scenario in this mode is that two adjacent coils are short circuited, thus this situation will be considered. The short-circuit condition should be paid attention. The objective function in this mode is given as

$$\text{Objective}: \ \min T_{ripple\_4} \tag{4}$$

where T_{ripple_4} is the torque ripple in mode 4.

5) *Mode 5*: High-speed operation

Since in this mode the net losses including copper loss and core loss has a major influence on the motor efficiency and the operation temperature, they have been selected as the objective. The objective function in this mode is given as

$$\text{Objective}: \ \min P_{loss\_5} \tag{5}$$

where P_{loss_5} is the loss in mode 5.

The angle position control (APC) method will be investigated for all the five driving modes since it is the commonly used control method for the SRM [13], [29].

D. Sensitivity analysis

For the simplification of the optimization process, a comprehensive sensitivity analysis is adopted to select the optimization variables and divide them into different subspaces [30]. The design variables are listed in Table II, and the sensitivity of f with regard to the parameter x_i can be given by

$$S(x_i) = \frac{V(E(f / x_i))}{V(f)} \tag{6}$$

where f is the optimization objective, $E(f/x_i)$ is the average value of f when x_i is constant, $V(E(f/x_i)$ is the variance of $E(f/x_i)$, and $V(f)$ is the overall variance of f.

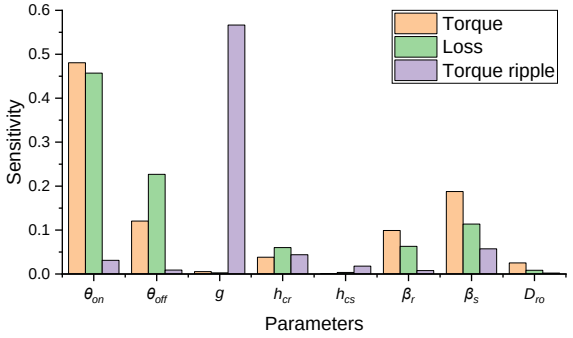

Fig. 5. Sensitivity indices for mode 1.

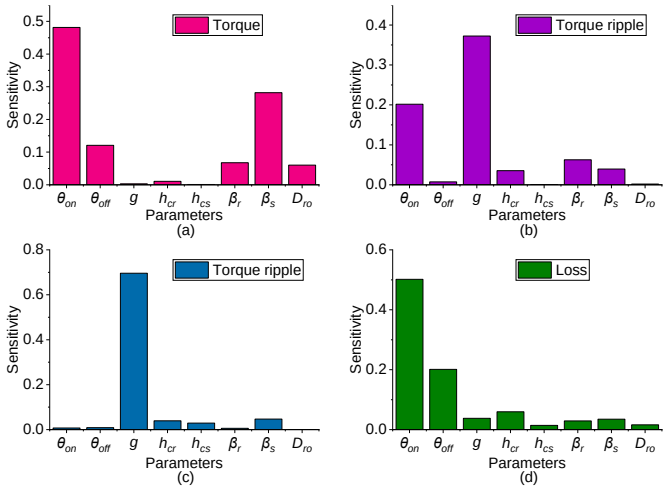

Fig. 6. Sensitivity indices (a)-(d) for modes 2-5.

Fig. 5 shows the sensitivity analysis results of the two control parameters and six geometry parameters for the three objectives in Mode 1. Besides, the sensitivity results of the other four driving modes are presented in Fig. 6. The sensitive variables can be identified from Figs. 5 and 6, and the results are shown in Table III. Besides, representative speeds of each mode are presented in Table III.

It can be found that one driving mode may have several influential variables and the same variable may significantly

affect the objectives of multiple driving modes. For example, there are four crucial variables in mode 1, i.e., θ_{on}, θ_{off}, g, and β_s, in which θ_{on} also shows high impact on the objectives of modes 2, 3 and 5. The crossover of the driving modes and their influential variables highly increase the difficulty of the optimization since different variables should be optimized for the driving modes. Taking the variables θ_{off} and g as an example, θ_{off} is important for modes 1, 2 and 5 while g has significant impact on the objectives of modes 1, 3 and 4. Thus, the selection of the optimal values of θ_{off} and g cannot be determined by the same driving modes. Thus, it is necessary to analyze the correlation of all the driving modes to further simplify the optimization process.

TABLE III
SELECTION OF SENSITIVE VARIABLES

Driving modes	Sensitive variables	Representative speed
Mode 1: Normal operation	θ_{on}, θ_{off}, g, β_s	$n = n_{\text{rated}}$
Mode 2: Start or climbing	θ_{on}, θ_{off}, β_s	$n \le 0.5n_{\text{rated}}$
Mode 3: Open circuit fault operation	θ_{on}, g	$n = n_{\text{rated}}$
Mode 4: Short circuit fault operation	g	$n = n_{\text{rated}}$
Mode 5: High speed operation	θ_{on}, θ_{off}	$n = 1.5\sim2n_{\text{rated}}$

TABLE IV
CORRELATION ANALYSIS OF OPTIMIZATION OBJECTIVES

	T_{avg_1}	P_{loss_1}	T_{ripple_1}	T_{avg_2}	T_{ripple_3}	T_{ripple_4}	P_{loss_5}
T_{avg_1}	1	*0.975*	0.215	0.992	0.368	0.128	*0.939*
P_{loss_1}	*0.975*	1	0.143	*0.960*	0.313	0.057	0.971
T_{ripple_1}	0.215	0.143	1	0.218	0.707	0.989	0.215
T_{avg_2}	0.992	*0.960*	0.218	1	0.373	0.134	*0.936*
T_{ripple_3}	0.368	0.313	0.707	0.373	1	0.661	0.355
T_{ripple_4}	0.128	0.057	0.989	0.134	0.661	1	0.135
P_{loss_5}	*0.939*	0.971	0.215	*0.936*	0.355	0.135	1

TABLE V
SELECTION OF OPTIMIZATION MODE AND OBJECTIVES

Optimization objectives	Optimization variables	Driving mode
T_{avg_1}	θ_{on}, θ_{off}, β_s	mode 1
P_{loss_1}	θ_{on}, θ_{off}, β_s	mode 1
T_{ripple_1}	g	mode 1
T_{ripple_3}	θ_{on}, g	mode 3

E. Correlation analysis

The Pearson correlation coefficients [31] between different optimization objectives in the five driving modes are calculated to show the relationship between the two objectives. The value close to 1 indicates a high correlation. It can be found in Table IV that T_{avg_1} and T_{avg_2} are in positive correlation since the Pearson correlation coefficient between the two objectives is 0.992, which is very close to 1. The same relationship can be found between P_{loss_1} and P_{loss_5}, and T_{ripple_1} and T_{ripple_4}, where the Pearson correlation coefficients are 0.971 and 0.989, respectively. Thus, the analysis of T_{avg_2}, P_{loss_5} and T_{ripple_4} can be substituted by T_{avg_1}, P_{loss_5} and T_{ripple_1}, respectively. It should be noted that in Table IV, although the Pearson correlation coefficient between T_{avg_1} and P_{loss_1} is 0.975 (similar between T_{avg_1} and P_{loss_5}, T_{avg_1} and P_{loss_1}, and T_{avg_2} and P_{loss_5}), since the optimization goal is to maximize the torque and minimize the loss, which means these are conflicting objectives, the analysis of the objectives related to loss cannot be substituted by the objectives related to torque. After the correlation analysis, only four objectives in two modes are selected for the optimization, as listed in Table V.

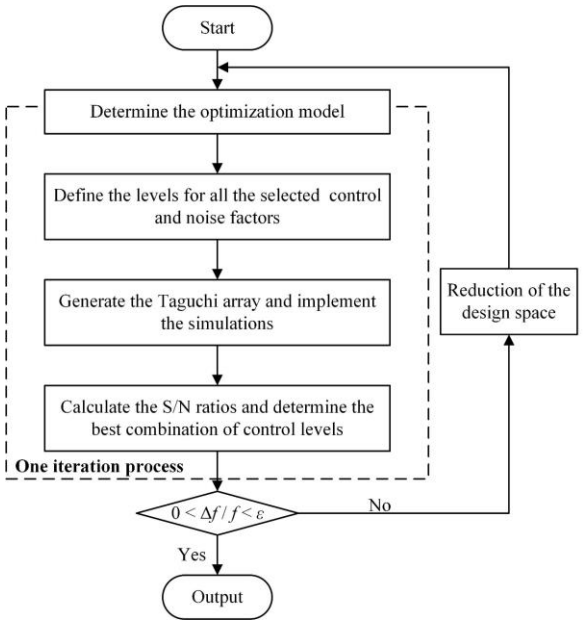

Fig. 7. Flowchart of the multilevel sequential Taguchi robust optimization method.

F. Sequential Taguchi method

Fig. 7 illustrates the flowchart of the multilevel sequential Taguchi robust optimization method. It can be divided into six steps.

Step 1: Determine the optimization model combining all the optimization objectives in the driving modes. The optimization model is defined as

$$\begin{aligned} \min: \quad & f(\mathbf{x}_s) = w_1 \frac{(T_{avg\_1})_{initial}}{T_{avg\_1}} + w_2 \frac{P_{loss\_1}}{(P_{loss\_1})_{initial}} \\ & + w_3 \frac{T_{ripple\_1}}{(T_{ripple\_1})_{initial}} + w_4 \frac{T_{ripple\_3}}{(T_{ripple\_3})_{initial}} \\ \text{s.t.} \quad & g_1(\mathbf{x}_s) = 0.85 - \eta \le 0 \\ & g_2(\mathbf{x}_s) = sf - 0.6 \le 0 \\ & g_3(\mathbf{x}_s) = J_c - 6.5 \le 0 \\ & \mathbf{x}_{sl} \le \mathbf{x}_s \le \mathbf{x}_{su} \end{aligned} \tag{7}$$

where $\mathbf{x}_s$, f, g_i are the design parameter vector, objective and constraints of motor, respectively, $\mathbf{x}_s$ consists of motor parameter vector and control parameter vector, $\mathbf{x}_{sl}$ and $\mathbf{x}_{su}$ are the lower boundary and upper boundary, respectively, η, sf and J_c (in A/mm^2) represent the efficiency, slot fill factor and current density, respectively, and w_1, w_2, w_3, and w_4 are the weighting factors. In this example, since T_{avg_1}, P_{loss_1}, and T_{ripple_1} are the representation of T_{avg_2}, P_{loss_5}, and T_{ripple_4}, respectively, the values of w_1, w_2, w_3, and w_4 are assigned as 2, 2, 2, and 1, respectively. The next several steps will constitute one iteration process, which is the main difference between the proposed sequential Taguchi method and the conventional Taguchi method.

TABLE VI
OPTIMIZATION VARIABLES AND RANGES

Parameter	Unit	Ranges
θ_{on}	deg.	[-6, -4]
θ_{off}	deg.	[9, 11]
β_s	deg.	[10, 14]
g	mm	[0.5, 1]

TABLE VII
LEVELS OF OPTIMIZATION VARIABLES

Variable	Level	Iteration 1	Iteration 2	Iteration 3	Iteration 4
θ_{on} (deg.)	1	-6	-5	-4.5	-4.25
	2	-5	-4.5	-4.25	-4.13
	3	**-4**	**-4**	**-4**	-4
θ_{off} (deg.)	1	**9**	9	9.5	9.75
	2	10	9.5	9.75	9.88
	3	11	**10**	**10**	10
β_s (deg.)	1	**10**	10	10.5	10.75
	2	12	**11**	**11**	11
	3	14	12	11.5	11.25
g (mm)	1	0.5	0.75	0.88	0.94
	2	0.75	0.88	0.94	0.97
	3	**1**	**1**	**1**	1

TABLE VIII
ORTHOGONAL ARRAY

No	θ_{on}	θ_{off}	β_s	g
1	3	2	3	1
2	3	3	1	2
3	2	1	3	2
4	2	3	2	1
5	2	2	1	3
6	1	3	3	3
7	1	1	1	1
8	3	1	2	3
9	1	2	2	2

Step 2: Define the levels for all the selected optimization variables and noise factors.

Table VI lists the optimization variables and their ranges. Tables VII lists the design levels of optimization variables for each iteration process, respectively. As shown, there are three levels for each optimization variable. The data in column Iteration 1 in Table VII represents the initial levels of each optimization variable. The selection of the levels in the other iteration process will be introduced in the next steps. Since there are no permanent magnets in SRMs, the air gap g is selected as the only noise factor and its design levels are set as -0.1 mm and +0.1 mm.

Step 3: Generate the orthogonal array based on the design levels of the control and noise factors, and implement the simulations according to the established array.

Table VIII lists the orthogonal array generated from these factors. As shown, it has nine rows defined by the optimization variables. 1, 2 and 3 in the table represent the indices of the corresponding levels presented in Table VII. During one iteration, 18 (9×2) combinations of FEM simulations will be performed to evaluate the performances in mode 1, and 6 (3×2) combinations of FEM analyses will be considered to determine the performances in mode 3. The reason why more samples are analyzed for mode 1 than for mode 3 is that there are four influential variables in mode 1 while only two in mode 3, as shown in Table V.

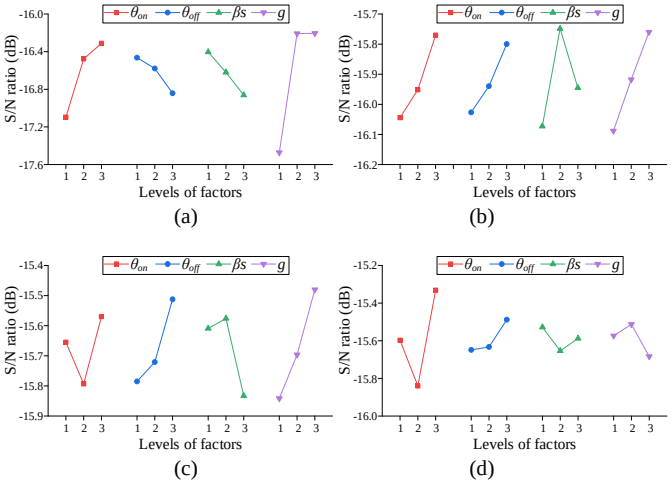

Fig. 8. Illustration of S/N ratios. (a) Iteration 1, (b) Iteration 2, (c) Iteration 3, and (d) Iteration 4.

Step 4: Calculate the S/N ratios and determine the best combination of design parameter levels for the optimization.

The calculation of the S/N ratios can be divided into two main steps: The first is to compute the S/N ratio for each row of the orthogonal array, and the respective equation is given by

$$SN(i) = -10 \times \lg[\frac{1}{2} \times \sum_{j=1}^{2} F^2(i, j)] \quad (8)$$

where i (1, 2, …, 9) and j (1, 2, 3, 4) are the row number in Table VIII and the index of the noise factor (variable), respectively.

Then, the average S/N ratios for all levels of optimization variables based on the S/N ratios of each row is computed. For example, the average S/N ratio for the first level of θ_{on} is the average value of $SN(6)$, $SN(7)$, and $SN(9)$. The combination of the best design levels for the optimization variables can be determined by the S/N ratios. The higher S/N ratio means the smaller F. Thus, the level of each optimization variable which reveals the highest S/N ratio is selected to determine the overall best design.

Fig. 8 presents the illustration of S/N ratios. As shown in Fig. 8(a), levels 3, 1, 1, and 3 are selected for θ_{on}, θ_{off}, g, and β_s, respectively, which correspond to -4, 9, 10, 1 in the column Iteration 1 in Table VII.

Step 5: Calculate the value of the selection criterion of the selected combination of design levels.

It should be noted that Steps 2~5 are considered as one iteration process. The idea for selecting a sequential iteration process is to further improve the performance and to make sure that the optimization process is converged and the performance of the identified optimal solution cannot be further improved.

Step 6: Termination judgement.

Compare the values of the selection criterion F between two successive iterations to judge whether the optimal solution meets the convergence condition. The value of F in iteration 1 should be compared with that of the initial design. If their

relative error is larger than 0 and smaller than a given value ε, terminate the iteration progress and output the optimal solution. Otherwise, reduce the design space and go to Step 2 to perform another iteration. It should be noted that if the relative error is completely equal to 0, it means the values for each control factor that were selected are the same. In this example, the value of ε is set as 3%.

The space reduction method is applied to reduce the design space, which is defined as follows. Assume the initial design space of an optimization variable is [a, b], and there are three levels with a step size d. It should be noted that the step size of each optimization variable will be halved during the space reduction. If the optimal value of this variable is x_0, then the design levels in the next iterative process will be determined by (9), where d in this formula is the step size of the present iteration.

$$\begin{cases} (a, a+d/2, a+d), & x_0 - d/2 < a \\ (b-d, b-d/2, b), & x_0 + d/2 > b \\ (x_0 - d/2, x_0, x_0 + d/2), & others \end{cases} \quad (9)$$

For example, for the variable θ_{on}, the best level is 3 in Iteration 1 and its corresponding value is -4º. As the step size in Iteration 1 is 1º, the next one is 0.5º. Thus, the next three levels in Iteration 2 will be -5, -4.5 and -4, respectively. The values of each level in each iteration process are listed in Table VII.

The illustration of S/N ratios of each iteration is presented in Fig. 8, and the best combination of optimization variables in each iteration is listed in Table IX, as well as the values of the objectives in each driving mode. It can be found in Figs. 8(b) and (c) that the same levels are selected in Iterations 2 and 3, which means the best combinations of the optimization variables in Iterations 2 and 3 are the same. The sequential Taguchi method will be terminated after four iterations. Since F of Iterations 2/3 achieves the lowest value, the optimal design is selected as the same with Iterations 2/3 listed in Table IX.

TABLE IX
PERFORMANCE COMPARISON

Parameter / Objective	Unit	Initial	Iteration 1	Iterations 2/3	Iteration 4
θ_{on}	deg.	-5	-4	-4	-4
θ_{off}	deg.	11	9	10	10
β_s	deg.	13.5	10	11	10.75
g	mm	0.5	1	1	0.97
T_{avg_1}	Nm	126.72	115.46	117.60	121.03
P_{loss_1}	kW	3.04	2.63	2.67	2.71
T_{ripple_1}	%	83.84	74.35	32.70	39.74
T_{avg_2}	Nm	462.58	420.89	449.65	460.43
T_{ripple_3}	%	170.32	162.66	138.72	142.57
T_{ripple_4}	%	83.08	75.60	33.27	40.30
P_{loss_5}	kW	2.44	1.83	1.92	1.94
f	-	7	6.65	5.51	5.66

Fig. 9 illustrates the flux density of the initial design and the optimal design at the aligned position when the two poles of one phase are excited with 50 A. In general, the optimal design exhibits lower values of flux density compared with the initial design. It means that the initial design is more likely to be saturated and the optimal design holds the stronger ability of output torque. It can be found in Table IX, the optimal solution achieved by the proposed optimization method can significantly reduce the torque ripples in modes 1, 3 and 4. Compared with the initial design, the torque ripples in mode 1, 3, and 4 can be reduced by about 60%, 18%, and 60%, respectively. Besides, although the torque in mode 1 is reduced by about 7%, the losses also be decreased by about 12%. As the definition of F is to evaluate the comprehensive performance of the SRM drive system considering multiple driving cycles, the comprehensive performance is improved by about 21%. Moreover, the torque curves of the initial design and optimal design in mode 1 and mode 3 are presented in Figs. 10 and 11, respectively. They illustrate the changes of torque and torque ripple more intuitively. Compared with mode 1, the value of minimum torque in mode 3 has been greatly reduced, since the open phase loses the ability to generate the force pulling the rotor from the unaligned position to the aligned position among the range of conduction angle.

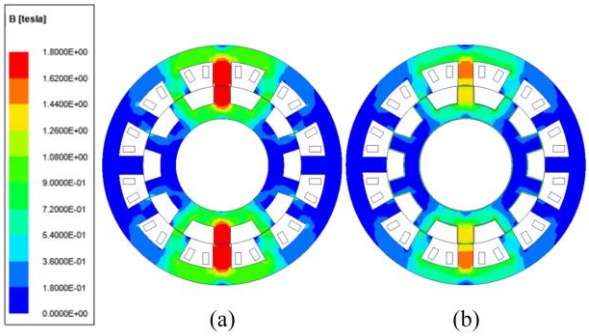

Fig. 9. Flux density at aligned position when the two stator poles of one phase are excited with 50 A. (a) Initial design and (b) Optimal design.

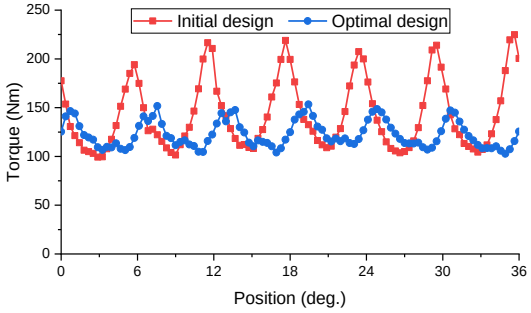

Fig. 10. Comparison of torque in mode 1.

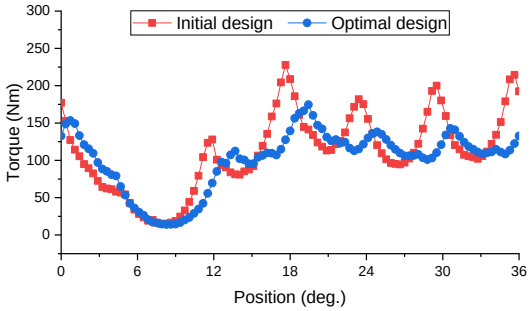

Fig. 11. Comparison of torque in mode 3.

IV. EXPERIMENTAL VALIDATION

In order to verify the accuracy of the simulation results and

the aforementioned analyses, the optimal design featuring 12 stator teeth and 10 rotor teeth is manufactured. Consequently, it is put into operation by using a test rig, as shown in Fig. 12. The whole motor drive is mounted onto a test bed, where the tested SRM, torque and speed sensor, and magnetic powder brake are connected by two couplings. A high-performance driving controller of dSPACE 1401 is employed to control the turn on and turn off angles of the APC method. The position signals are detected by the Hall sensor ATS675LSE.

Fig. 13 shows the measured current waveforms of the normal operation and open circuit fault conditions. The motor first operates under the normal operation, then an open-circuit fault occurs in phase C. It can be observed that the open-circuit fault of phase C does not influence the current of the other phases, which reveals the high tolerance ability of SRMs. Figs. 14 and 15 illustrate the comparison of the torque derived by simulations and experiments for mode 1 and mode 3, respectively. The average errors for mode 1 and mode 3 considering the difference of the simulation and experimental results are no more than 3% and 5%, respectively.

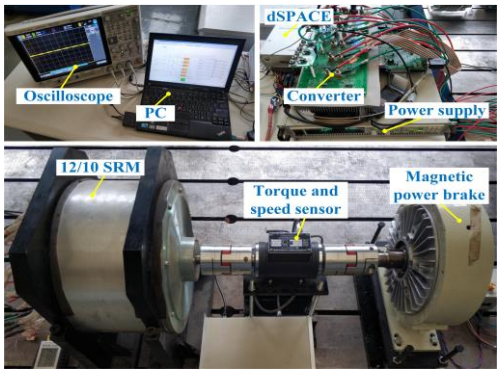

Fig. 12. Experimental platform of the 12/10 SRM drive system.

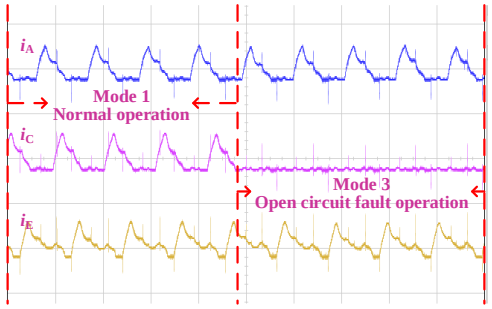

Fig. 13. Measured current waveforms.

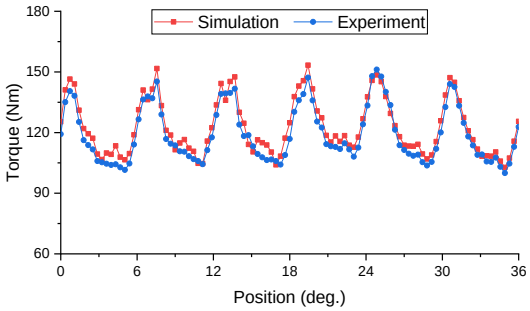

Fig. 14. Torque comparison between simulation and experiments for mode 1.

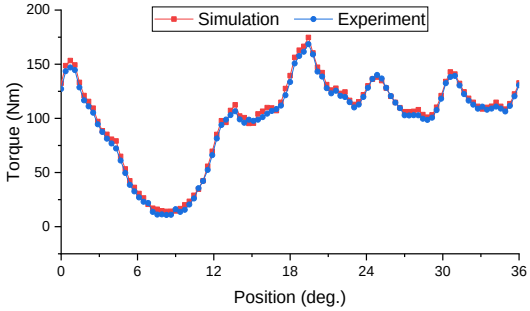

Fig. 15. Torque comparison between simulation and experiments for mode 3.

V. Conclusion

In this paper, a novel system-level robust design optimization considering multiple driving modes was proposed for a 12/10 SRM drive system considered for electric vehicle application. Five driving modes of the motor system were defined according to the considered driving cycle. To improve the optimization efficiency, a sensitivity analysis was implemented to identify influential variables as the design parameters for the optimization. A correlation analysis was implemented to determine the coherence of the objective functions of all driving modes in order to simplify the optimization process. Moreover, a sequential Taguchi method was proposed and applied to search for the optimal solution. A selection criterion was defined and the iterative process was terminated as the value of the selection criterion converged. The simulation results and a consequent experimental validation revealed that the proposed method allows to significantly reducing the torque ripple and improving the overall performance of the SRM.

References

[1] P. J. d. S. Neto, T. A. d. S. Barros, M. V. d. Paula, R. R. d. Souza, and E. R. Filho, "Design of computational experiment for performance optimization of a switched reluctance generator in wind systems," *IEEE Trans. Energy Convers.*, vol. 33, no. 1, pp. 406-419, 2018.

[2] X. Sun, K. Diao, G. Lei, Y. Guo, and J. Zhu, "Real-time HIL emulation for a segmented-rotor switched reluctance motor using a new magnetic equivalent circuit," *IEEE Trans. Power Electron.*, vol. 35, no. 4, pp. 3841-3849, 2020.

[3] W. Uddin, T. Husain, Y. Sozer, and I. Husain, "Design methodology of a switched reluctance machine for off-road vehicle applications," *IEEE Trans. Ind. Appl.*, vol. 52, no. 3, pp. 2138-2147, 2016.

[4] J. D. Widmer, R. Martin, and B. C. Mecrow, "Optimization of an 80-kW segmental rotor switched reluctance machine for automotive traction," *IEEE Trans. Ind. Appl.*, vol. 51, no. 4, pp. 2990-2999, 2015.

[5] K. Kiyota, T. Kakishima, and A. Chiba, "Comparison of test result and design stage prediction of switched reluctance motor competitive with 60-kW rare-earth PM motor," *IEEE Trans. Ind. Electron.*, vol. 61, no. 10, pp. 5712-5721, 2014.

[6] K. Diao, X. Sun, G. Lei, Y. Guo, and J. Zhu, "Multiobjective system level optimization method for switched reluctance motor drive systems using finite element model," *IEEE Trans. Ind. Electron.*, 2020.

[7] X. Sun, Z. Shi, Y. Cai, G. Lei, Y. Guo, and J. Zhu, "Driving-cycle oriented design optimization of a permanent magnet hub motor drive system for a four-wheel-drive electric vehicle," *IEEE Trans. Transport. Electrific.*, 2020.

[8] X. Zhu, W. Wu, L. Quan, Z. Xiang, and W. Gu, "Design and multi-objective stratified optimization of a less-rare-earth hybrid permanent magnets motor with high torque density and low cost," *IEEE Trans. Energy Convers.*, vol. 34, no. 3, pp. 1178-1189, 2019.

[9] X. Sun, K. Diao, G. Lei, Y. Guo, and J. Zhu, "Study on segmented-rotor

switched reluctance motors with different rotor pole numbers for BSG system of hybrid electric vehicles," *IEEE Trans. Veh. Technol.*, vol. 68, no. 6, pp. 5537-5547, 2019.
[10] Z. Shi, X. Sun, Y. Cai, and Z. Yang, "Robust design optimization of a five-phase PM hub motor for fault-tolerant operation based on Taguchi method," *IEEE Trans. Energy Convers.*, 2020.
[11] H. Chen, W. Yan, J. J. Gu, and M. Sun, "Multiobjective optimization design of a switched reluctance motor for low-speed electric vehicles with a Taguchi–CSO algorithm," *IEEE/ASME Trans. Mechatron.*, vol. 23, no. 4, pp. 1762-1774, 2018.
[12] E. Öksüztepe, "In-wheel switched reluctance motor design for electric vehicles by using a Pareto-based multiobjective differential evolution algorithm," *IEEE Trans. Veh. Technol.*, vol. 66, no. 6, pp. 4706-4715, 2017.
[13] X. Sun, K. Diao, G. Lei, Y. Guo, and J. Zhu, "Direct torque control based on a fast modeling method for a segmented-rotor switched reluctance motor in HEV application," *IEEE J. Emerg. Sel. Topics Power Electron.*, 2020.
[14] X. Sun, K. Diao, and Z. Yang, "Performance improvement of a switched reluctance machine with segmental rotors for hybrid electric vehicles," *Comput. Electr. Eng.*, vol. 77, pp. 244-259, 2019.
[15] G. Lei, T. Wang, Y. Guo, J. Zhu, and S. Wang, "System-level design optimization methods for electrical drive systems: deterministic approach," *IEEE Trans. Ind. Electron.*, vol. 61, no. 12, pp. 6591-6602, 2014.
[16] B. Ma, G. Lei, J. Zhu, Y. Guo, and C. Liu, "Application-oriented robust design optimization method for batch production of permanent-magnet motors," *IEEE Trans. Ind. Electron.*, vol. 65, no. 2, pp. 1728-1739, 2018.
[17] X. Zhu, Z. Xiang, C. Zhang, L. Quan, Y. Du, and W. Gu, "Co-reduction of torque ripple for outer rotor flux-switching PM motor using systematic multi-level design and control schemes," *IEEE Trans. Ind. Electron.*, vol. 64, no. 2, pp. 1102-1112, 2017.
[18] C. Liu, G. Lei, B. Ma, Y. Guo, and J. Zhu, "Robust design of a low-cost permanent magnet motor with soft magnetic composite cores considering the manufacturing process and tolerances," *Energies*, vol. 11, no. 8, 2018.
[19] S. Lee, K. Kim, S. Cho, J. Jang, T. Lee, and J. Hong, "Optimal design of interior permanent magnet synchronous motor considering the manufacturing tolerances using Taguchi robust design," *IET Elect. Power Appl.*, vol. 8, no. 1, pp. 23-28, 2014.
[20] G. Lei, T. Wang, J. Zhu, Y. Guo, and S. Wang, "System-level design optimization method for electrical drive systems—robust approach," *IEEE Trans. Ind. Electron.*, vol. 62, no. 8, pp. 4702-4713, 2015.
[21] J. Song, F. Dong, J. Zhao, S. Lu, S. Dou, and H. Wang, "Optimal design of permanent magnet linear synchronous motors based on Taguchi method," *IET Elect. Power Appl.*, vol. 11, no. 1, pp. 41-48, 2017.
[22] K. Kim, K. Jung, J. Kim, J. Hong, and S. Kim, "Taguchi robust optimum design for reducing the cogging torque of EPS motors considering magnetic unbalance caused by manufacturing tolerances of PM," *IET Elect. Power Appl.*, vol. 10, no. 9, pp. 909-915, 2016.
[23] X. D. Xue, K. W. E. Cheng, T. W. Ng, and N. C. Cheung, "Multi-objective optimization design of in-wheel switched reluctance motors in electric vehicles," *IEEE Trans. Ind. Electron.*, vol. 57, no. 9, pp. 2980-2987, 2010.
[24] X. Zhu, Z. Xiang, L. Quan, W. Wu, and Y. Du, "Multimode optimization design methodology for a flux-controllable stator permanent magnet memory motor considering driving cycles," *IEEE Trans. Ind. Electron.*, vol. 65, no. 7, pp. 5353-5366, 2018.
[25] Z. Shi, X. Sun, Y. Cai, X. Tian, and L. Chen, "Design optimization of an outer-rotor permanent magnet synchronous hub motor for a low-speed campus patrol EV," *IET Electr. Power Appl.*, 2020
[26] P. Lazari, J. Wang, and L. Chen, "A computationally efficient design technique for electric-vehicle traction machines," *IEEE Trans. Ind. Appl.*, vol. 50, no. 5, pp. 3203-3213, 2014.
[27] Z. Yang, F. Shang, I. P. Brown, and M. Krishnamurthy, "Comparative study of interior permanent magnet, induction, and switched reluctance motor drives for EV and HEV applications," *IEEE Trans. Transport. Electrific.*, vol. 1, no. 3, pp. 245-254, 2015.
[28] M. Degano, E. Carraro, and N. Bianchi, "Selection criteria and robust optimization of a traction PM-assisted synchronous reluctance motor," *IEEE Trans. Ind. Appl.*, vol. 51, no. 6, pp. 4383-4391, 2015.
[29] W. Ding, S. Yang, and Y. Hu, "Performance improvement for segmented-stator hybrid-excitation SRM drives using an improved asymmetric half-bridge converter," *IEEE Trans. Ind. Electron.*, vol. 66, no. 2, pp. 898-909, 2019.
[30] X. Zhu, J. Huang, L. Quan, Z. Xiang, and B. Shi, "Comprehensive sensitivity analysis and multiobjective optimization research of permanent magnet flux-intensifying motors," *IEEE Trans. Ind. Electron.*, vol. 66, no. 4, pp. 2613-2627, 2019.
[31] X. Sun, Z. Shi, G. Lei, Y. Guo, and J. Zhu, "Multi-objective design optimization of an IPMSM based on multilevel strategy," *IEEE Trans. Ind. Electron.*, 2020.

Kaikai Diao (S'18) was born in Zhenjiang, Jiangsu, China, in 1994. He received the B.S. degree in vehicle engineering from Jiangsu University, Zhenjiang, China, in 2017, and he is currently working toward the Ph.D. degree in Jiangsu University, Zhenjiang, China.

His current research interests include design, optimization, magnetic equivalent circuits modeling, control, and loss analysis of switched reluctance motors for automobile application.

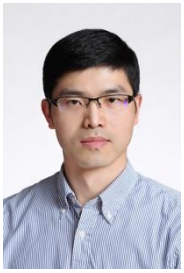

Xiaodong Sun (M'12-SM'18) received the B.Sc. degree in electrical engineering, and the M.Sc. and Ph.D. degrees in control engineering from Jiangsu University, Zhenjiang, China, in 2004, 2008, and 2011, respectively.

Since 2004, he has been with Jiangsu University, where he is currently a Professor with the Automotive Engineering Research Institute. From 2014 to 2015, he was a Visiting Professor with the School of Electrical, Mechanical, and Mechatronic Systems, University of Technology Sydney, Sydney, Australia. His current teaching and research interests include electrical machines and drives, drives and control for electric vehicles, and intelligent control. He is the author or coauthor of more than 80 refereed technical papers and one book, and he is the holder of 36 patents in his areas of interest.

Gang Lei (M'14) received the B.S. degree in Mathematics from Huanggang Normal University, China, in 2003, the M.S. degree in Mathematics and Ph.D. degree in Electrical Engineering from Huazhong University of Science and Technology, China, in 2006 and 2009, respectively.

He is currently a Senior Lecturer at the School of Electrical and Data Engineering, University of Technology Sydney (UTS), Australia. His research interests include computational electromagnetics, design optimization and control of electrical drive systems and renewable energy systems. He is an Associate Editor of the IEEE TRANSACTIONS ON INDUSTRIAL ELECTRONICS.

Gerd Bramerdorfer (S'10-M'14-SM'18) received the Ph.D. degree in electrical engineering from Johannes Kepler University Linz, Linz, Austria, in 2014. He is currently an Assistant Professor with the Department of Electrical Drives and Power Electronics, Johannes Kepler University Linz. His research interests include the design, modeling, and optimization of electric machines as well as magnetic bearings and bearingless machines.

Dr. Bramerdorfer is a Senior Member of IEEE, an Editor of the IEEE TRANSACTIONS ON ENERGY CONVERSION and a past Associate Editor of the IEEE TRANSACTIONS ON INDUSTRIAL ELECTRONICS.

Youguang Guo (S'02-M'05-SM'06) received the B.E. degree from Huazhong University of Science and Technology, China in 1985, the M.E. degree from Zhejiang University, China in 1988, and the Ph.D. degree from University of Technology, Sydney (UTS), Australia in 2004, all in electrical engineering.

He is currently a Professor at the School of Electrical and Data Engineering, University of Technology Sydney (UTS). His research fields include measurement and modeling of properties of magnetic materials, numerical analysis of electromagnetic field, electrical machine design optimization, power electronic drives and control.

Jianguo Zhu (S'93–M'96–SM'03) received the B.E. degree in 1982 from Jiangsu Institute of Technology, Jiangsu, China, the M.E. degree in 1987 from Shanghai University of Technology, Shanghai, China, and the Ph.D. degree in 1995 from the University of Technology Sydney (UTS), Sydney, Australia, all in electrical engineering.

He was appointed a lecturer at UTS in 1994 and promoted to full professor in 2004 and Distinguished Professor of Electrical Engineering in 2017. At UTS, he has held various leadership positions, including the Head of School for School of Electrical, Mechanical and Mechatronic Systems and Director for Centre of Electrical Machines and Power Electronics. In 2018, he joined the University of Sydney, Australia, as a full professor and Head of School for School of Electrical and Information Engineering. His research interests include computational electromagnetics, measurement and modelling of magnetic properties of materials, electrical machines and drives, power electronics, renewable energy systems and smart micro grids.